*J Mater Sci* (2018) 53:1318–1325

Energy materials

# Yolk-shell structured $Cu_2O$ as a high-performance cathode catalyst for the rechargeable Li-$O_2$ batteries

Xiao-yang Qiu[1,*], Shu-juan Liu[1], and Deng-zhu Xu[1]

[1] College of Science and Technology, Ningbo University, Ningbo 315212, People's Republic of China

**Received:** 22 July 2017
**Accepted:** 4 September 2017
**Published online:** 11 September 2017



## ABSTRACT

Developing an efficient cathode catalyst material is the most intrinsic requisite to acquire rechargeable Li-$O_2$ batteries with long cycling life and high rate capacity. Here, yolk-shell structured $Cu_2O$ spheres were facilely synthesized using a wet-chemistry method with the PEG-500 as the surfactant. As catalyst cathode materials, yolk-shell structured $Cu_2O$ spheres show a low discharge/charge potential platform of 1.28 V with current density of 500 mA $g^{-1}$. Compared with cubic-like $Cu_2O$ nanoparticles, yolk-shell structured $Cu_2O$ spheres have indicated a long and stable cycling life of 84 cycles with a high current density of 500 mA $g^{-1}$, and which may be benefited to the porous structure and the large specific surface area. The introduction of $Cu_2O$ provides an effective solution to the problem of low round-trip efficiency in the Li-$O_2$ battery.

## Introduction

With the rapid development of electric vehicles and mobile electronic devices, it is expected that the energy storage system can match their requirement with ultrahigh energy density, superior safety, low cost, as well as long and stable cycle life. Although they have been serving for energy storage and conversion for many years, the rechargeable lithium-ion batteries cannot meet the superhigh energy density (up to 500 Wh $kg^{-1}$) requirement of modern electronic devices with the primary and most fundamental limitation of intercalation chemistry. Recently, with a superhigh theoretical energy density about 3500 W h $kg^{-1}$, the lithium-oxygen batteries, with a Li anode and $O_2$ (which is ideally from the atmosphere) as the cathode, have been extensive addressed not only on the academic research but also in the technological application [1–3]. As the basic reaction between the lithium ion and the oxygen ($2Li^+ + O_2 + 2e^- = Li_2O_2$), it is indicated that the Li-$O_2$ batteries system does not need any heavy transition metals or intercalation frameworks besides the superhigh energy density [4–7]. Moreover, it is well known that oxygen is a limitless, non-toxic and non-polluting material which makes Li-$O_2$ energy storage system more appealing as the next-generation energy storage system. Nevertheless, accompanying the innovation processes of the Li-$O_2$ batteries system, several critical issues which must be settled have plagued its practical application seriously. Among them, the most important obstacle is the large overpotential, which leads to the lower coulombic efficiency. Recent research indicates that the over-

Address correspondence to E-mail: 15958867884@163.com



DOI 10.1007/s10853-017-1555-y

potential of the Li-$O_2$ batteries can be reduced efficiently by using some electrocatalyst, and the rate performance and the capacity can be improved with appropriate electrocatalyst also. [8–10] Various kinds of electrocatalyst have been explored to improve the catalytic activities for the Li-$O_2$ batteries, such as the noble metals, [11] carbon materials, [12] and transition metal compounds [13–15].

Among numerous transition metal oxides, cuprous oxide a p-type semiconductor has been noted for the remarkable potential application in the catalysis, anode materials for the lithium-ion batteries and solar cell materials for solar energy conversion [16, 17]. Its widely application may be attributed to its own properties—non-toxic, environmentally friendly and abundant in nature. It is generally known that the physical or chemical properties will be affected by the morphology of the nanomaterials. Thus the $Cu_2O$ materials have been morphology-controlled synthesis with different micro/nanostructure such as hollow spheres, core–shell spheres and porous particles [18–20]. Here, yolk-shelled structured $Cu_2O$ were synthesized by a gentle method with the polyethylene glycol (PEG) as surfactant, and the catalytic activity as a cathode material for Li–$O_2$ batteries has been studied.

## Experiment details

### Synthesis and characterization of yolk-shell structured $Cu_2O$

All the analytically pure chemical reagents used in this experiment were bought from the Sinopharm Chemical Reagent Co., Ltd (SCRC) and without any further purification. And here, the polyethylene glycol (PEG) with the molecular weight of 500 is abbreviated as PEG-500 in this manuscript. Typically, 100 ml $Cu(CH_3COO)_2{\cdot}H_2O$ (0.75 M/L) mixed with various dosages of PEG-500 was dissolved into 100 ml DI water to form the homogeneous solution. Next, the mixed solution was in reaction with the 50 °C oil bath and stirred with a fixed speed of about 400 r/min. Subsequently, 10 mL of NaOH (1 mol/L) was dripped into the mixed solution, and 20 mL of ascorbic acid (0.5 mol/L) was added drop by drop after 3 min. The whole reaction was kept at about 50 °C for two hours. The final product was collected after centrifugation and the wash process with the ethanol and the DI water for several times. Then, the $Cu_2O$ powder was dried at about 40 °C for 10 h in the vacuum drying chamber.

The crystal structure of the final product $Cu_2O$ powder was tested with the X-ray diffraction (XRD) pattern; the microstructure and the morphology of the $Cu_2O$ powder were investigated by the scanning electron microscope (SEM) and transmission electron microscopy (TEM) measurements.

### Assembly of the cell and electrochemical measurements

Here, 2032 type coin cells were assembled to form the Li-$O_2$ batteries and lithium metal was used as the counter electrode. Slurry which is comprised of active materials (as in this manuscript the $Cu_2O$ powder is used), and Ketjen carbon (KB) and polyvinylidene difluoride (PVDF) with the weight ratio of 6:3:1 were pasted on a carbon paper. Then the pasted carbon paper with the mass loading of the $Cu_2O$/KB/PVDF about 1.0–1.2 mg $cm^{-2}$ was dried at 60 °C in a vacuum chamber for 10 h. 1 M LITFSI (lithium bis-(trifluoromethanesulfonyl)-imide) in TEGDME (tetraethylene glycol dimethyl ether) was used as the electrolyte, and 100 uL was enough for one cell. With the glass filter paper used as the separator, the batteries were assembled in the glove box (< 0.1 ppm of $H_2O$ and 0.1 ppm of $O_2$). Finally, the assembled Li-$O_2$ batteries were transferred into a box which was filled with high pure oxygen (99.999%) for the electrochemical test.

Electrochemical impedance spectroscopy investigations were done on an Autolab 1.9 electrochemistry workstation. The NEWARE battery test system was used to test the galvanostatic discharge/charge capacities at different current densities in the potential range of 2.0–5.0 V. The galvanostatic discharge/charge test was based on the mass of KB.

## Results and discussion

Figure 1 indicates the XRD pattern of the product which was synthesized with 0 g (black line) and 0.3 g PEG-500 as the surfactant (red line). It can be seen that the diffraction peaks at about 36.52, 42.41, 61.42 and 73.60 2-theta degree are matched to the (111), (200) (220) and (311) lattice planes of the cubic phase of $Cu_2O$ (PDF#65-3288), respectively. The XRD

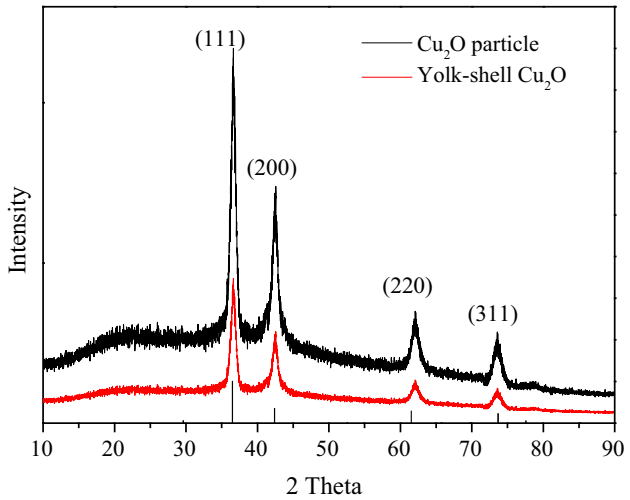


**Figure 1** XRD pattern of the product obtained with the surfactant of 0 g (black line) and 0.3 g PEG-500 (red line).

pattern also shows a good crystalline about the synthesized product, and there was no diffraction peak of impurity detected, which indicates the high purity of the synthesized $Cu_2O$ powder. If we change the amounts of the PEG-500 to 0.1, 0.5, 0.7 and 1.0 g, respectively, in our experiment, the same XRD pattern result could be obtained and only the intensity of the diffraction peaks changed a little.

Figure 2 indicates the SEM and the TEM images of the synthesized $Cu_2O$ powder with 0 g (a) and 0.3 g (b, c and d) PEG-500 as the surfactants. The SEM results (as shown in Fig. 2a) indicate that the sample which was synthesized without the surfactant shows a cubic-like particles surface morphology with the size around 50 nm. But things changed absolutely when the surfactant was added in the reaction. Even with about 0.1 g PEG-500, the product indicated a changed trend from the cubic-like particles to the spherical-like structures. Figure 2b, c and d indicates SEM and TEM images of the yolk-shell structured $Cu_2O$ spheres. From Fig. 2(b & c), the uniform spheres can be detected and the sizes are much bigger than the cubic-like particles, and it can be seen that the spheres were assembled from many small

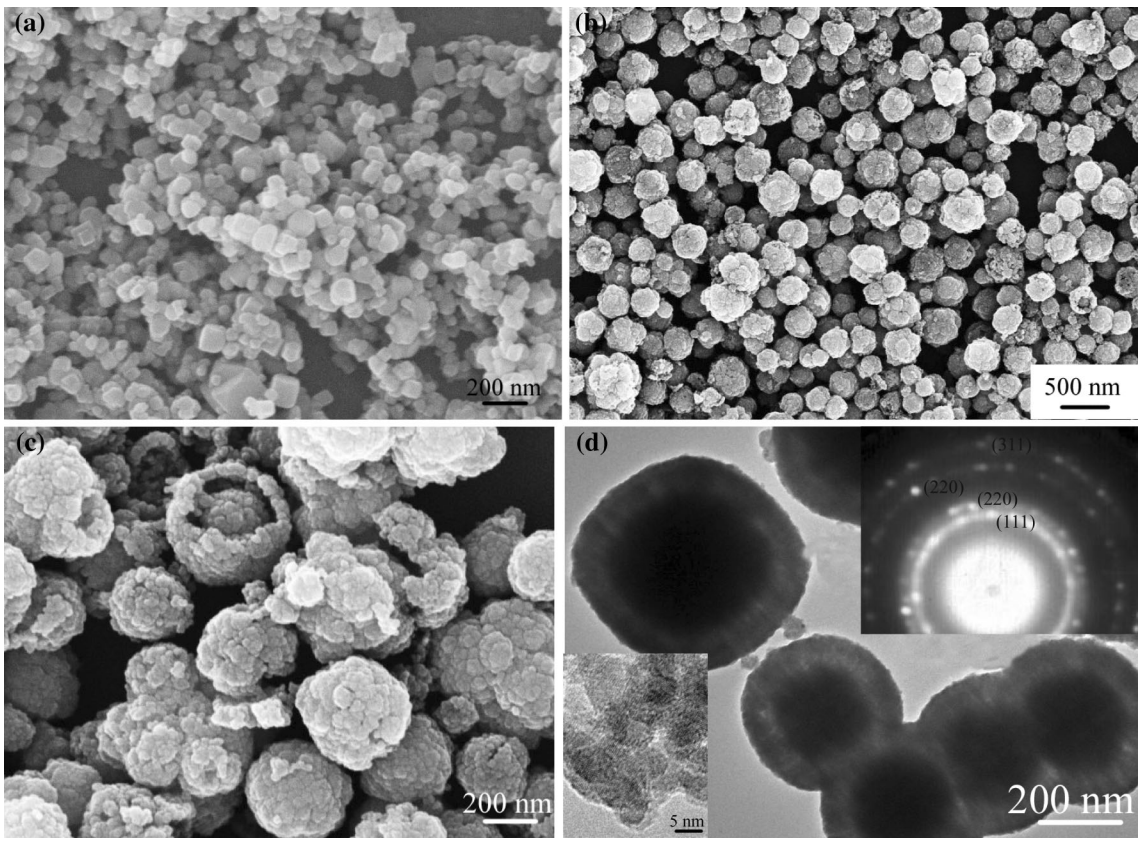


**Figure 2** **a** and **b** shows the SEM images of the products obtained at 0 g (**a**), 0.3 g (**b**), PEG-500, respectively. Figure 2c and d indicates the yolk-shell structure of the $Cu_2O$ synthesized with 0.3 g PEG-500. And the inset in the Fig. 2d shows the HRTEM image and SAED pattern of these $Cu_2O$ slices.

particles. The broken spheres can be detected in the Fig. 2b, which has been zoomed in and shown in Fig. 2c, where the yolk-shell structure of the $Cu_2O$ can be detected directly. The TEM image in Fig. 2d can further determine the yolk-shell structure of the $Cu_2O$ sphere. The inset HRTEM picture at the lower-left corner confirms that there are many small $Cu_2O$ particles assembled to form the sphere. And the selected-area electron diffraction (SAED) pattern which was the inset in the top-right corner shows the diffraction rings which were made up of many diffraction spots, indicating the polycrystalline structure of the synthesized $Cu_2O$ spheres. The samples which were synthesized with various surfactants (0.1, 0.5, 0.7 and 1.0 g PEG-500, respectively) exhibited the seam results except the sphere sizes and uniform. The forming of the yolk-shell structured $Cu_2O$ spheres may be attributed to the mechanism of Ostwald ripening and the effect of the surfactant (the ascorbic acid and the PEG-500) [19].

The synthesized yolk-shell structured $Cu_2O$ spheres were characterize by the manful XPS method which can locate the valence of the d orbital about the transiting metal compound easily. The full spectrum of the yolk-shell structured $Cu_2O$ synthesized with 0.3 g surfactant is shown in Fig. 3a. In Fig. 3b, the two peaks at about 952.1 and 932.3 eV are corresponding to the $Cu2p_{1/2}$ and $Cu2p_{3/2}$ characteristic peaks, respectively [19, 21]. And here, the O1 s peak can be detected at about 530.6 eV which is in conformity to the approximate value in the references [19, 22].

An $N_2$ adsorption–desorption isotherm was utilized to imply further details about the different structures of the surface area of the $Cu_2O$. The results indicate that the specific surface area of the yolk-shell structured $Cu_2O$ spheres reaches 179 $m^2\ g^{-1}$, which is much bigger than that of the cubic-like $Cu_2O$ nanoparticles (around 95 $m^2\ g^{-1}$). The BJH pore size distribution curves (the inset in Fig. 4) indicate the average aperture of the yolk-shell structured $Cu_2O$ spheres is mainly about 10 nm, which may provide more electrochemical active sites and channels for diffusion of the electrolyte, leading to outstanding electrochemical properties as a result.

The electrocatalytic properties of the cubic-like $Cu_2O$ nanoparticles and the yolk-shell structured $Cu_2O$ spheres were detected as the cathode catalyst of the lithium-oxygen batteries. The original cycle with the discharge/charge current density about 100, 200

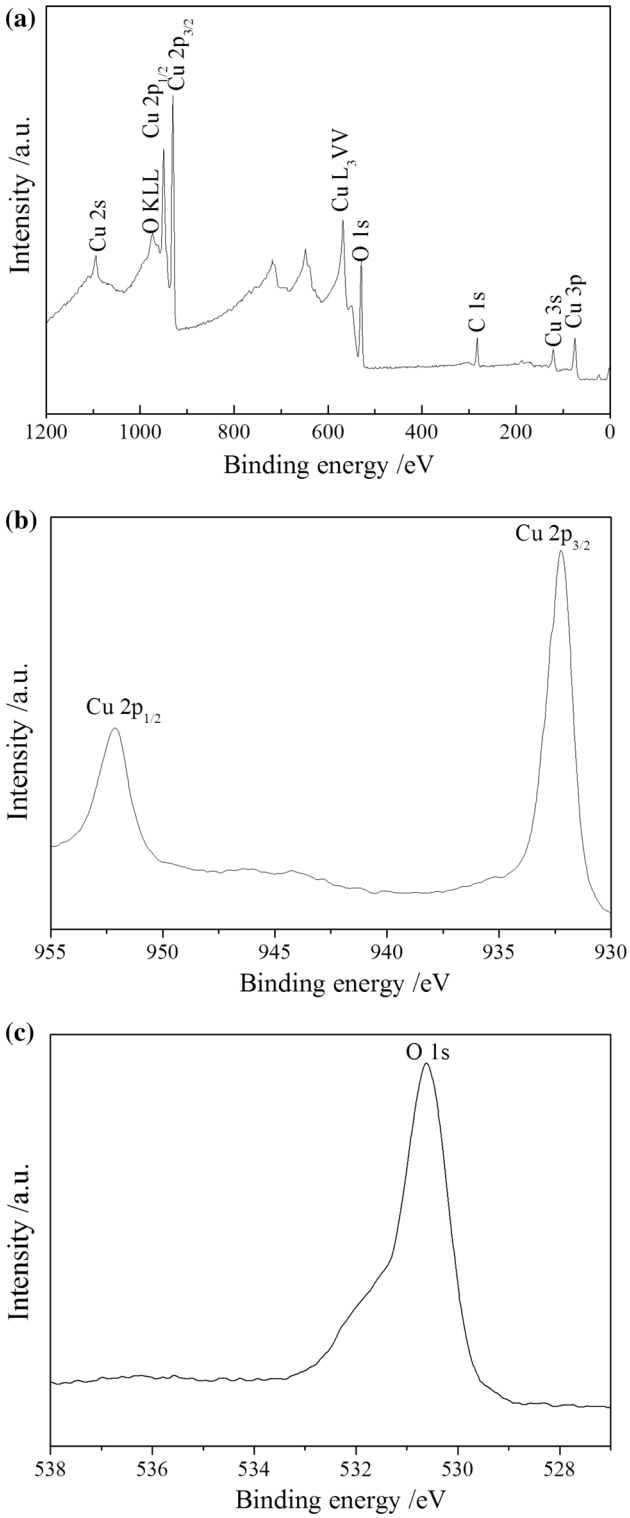


**Figure 3** Survey of XPS spectra of the $Cu_2O$ sphere **a** and the magnified XPS spectra **b** and **c** with the exact positions of the Cu2p and O1 s peaks, respectively.

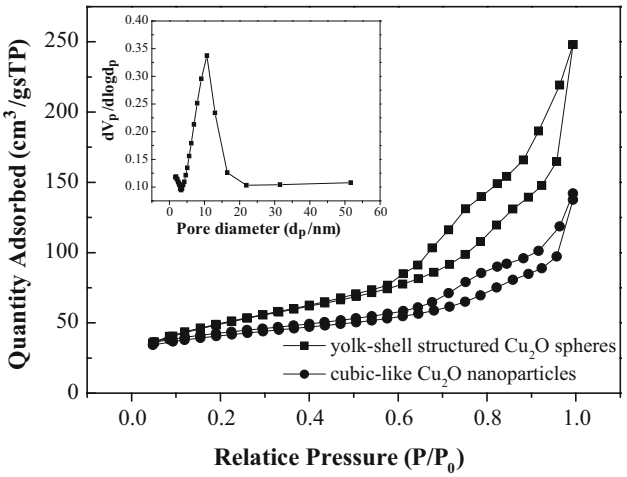


**Figure 4** $N_2$ adsorption–desorption isotherm and pore size distribution curve (inset) of the synthesized $Cu_2O$.

and 500 mA $g^{-1}$ of the yolk-shell Cu2O spheres as the catalytic materials is displayed in Fig. 5a. In contrast to the much alike curves during the discharge process, it can be seen that the charge process presented a different curve and the curve changed with various current densities. The over-potential platform was very low in our experiment, and the value was about 1.10 V with the discharge/charge current density about 100 and 200 mA $g^{-1}$. The over-potential platform just displayed as 1.28 V even with the extremely high current density of 500 mA $g^{-1}$. The lower over-potential revealed the outstanding catalytic activity and electrochemical stability for the oxygen reduction reaction (ORR) and oxygen evolution reaction (OER) [1, 2, 6, 14, 23, 24]. There the cubic-like $Cu_2O$ nanoparticles revealed an approximately good result. The discharge/charge performance of the yolk-shell

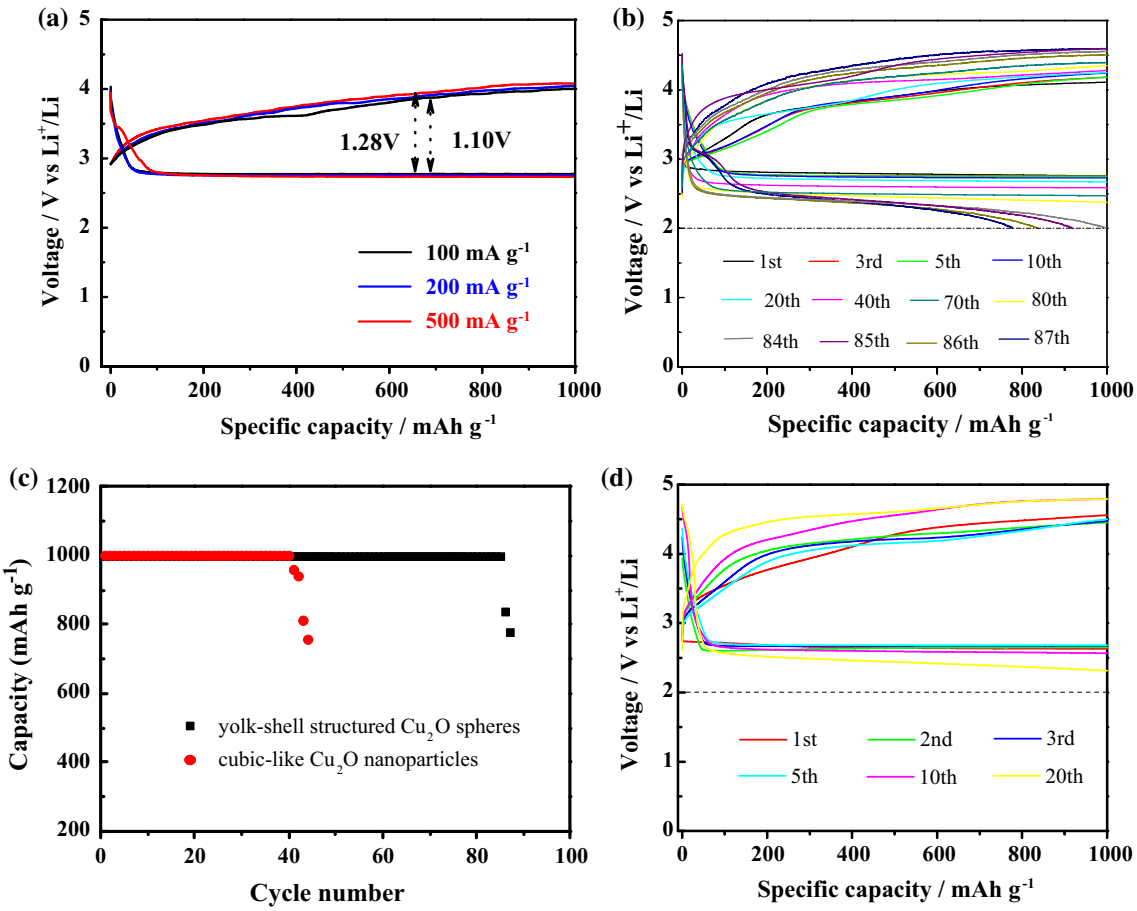


**Figure 5** Discharge/charge curves of Li-$O_2$ batteries assembled with the $Cu_2O$ as the catalyst for the cathodes materials with the current densities of **a** 100, 200 and 500 mA $g^{-1}$ for the first cycle and **b** with the current density about 500 mA $g^{-1}$ for subsequent cycles. **c** The cycle number of the yolk-shell structured and cubic-like $Cu_2O$ materials as the cathodes materials with the current density about 500 mA $g^{-1}$ with a limited capacity of 1000 mA h $g^{-1}$. **d** The cycle performance of the Li-$O_2$ batteries with the Ketjen carbon (KB) as the catalyst for the cathodes materials.

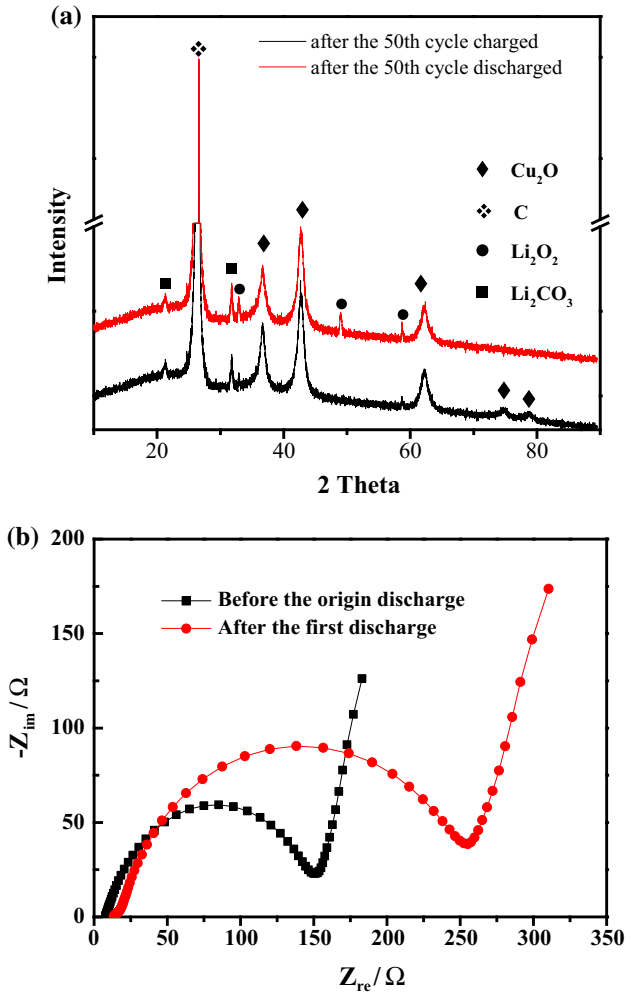


**Figure 6** **a** shows the XRD spectra of the yolk-shell structured $Cu_2O$ spheres after the 50th discharge/charge as the catalyst activity materials for the Li-$O_2$ batteries, respectively. And the EIS patterns before/after the original cycle were displayed in the Fig. 6b.

structured $Cu_2O$ cathodes with a limited capacity about 1000 mAh $g^{-1}$ at the higher current density of 500 mA $g^{-1}$ is displayed in Fig. 5b. When the discharge/charge performance reached the 84th cycle, the discharge potential got the cutoff potential of 2 V. And in the following discharge, they did not get the limited capacity because of the cutoff potential limit. This phenomenon was mainly caused by the decomposition and accumulation of the binder and electrolyte during the cycles [14, 25]. The cycle number of the yolk-shell structured and cubic-like $Cu_2O$ for 500 mA $g^{-1}$ with a limited capacity of 1000 mAh $g^{-1}$ is shown in Fig. 5c. It can be seen that the cubic-like $Cu_2O$ nanoparticles as the cathode catalyst with the limited capacity of 1000 mAh $g^{-1}$ demonstrated 40 full discharge/charge cycles only, but the yolk-shell structured $Cu_2O$ sphere indicated 84 full cycles. Compared with the cubic-like $Cu_2O$ nanoparticles, the fascinating cycle performance of the yolk-shell structure $Cu_2O$ sphere was mainly attributed to the super big specific spherical surface area and the porous structure which provided more active sites and more pathways for the lithium ions and oxygen. Figure 5d shows the cycle performance of the Li-$O_2$ batteries with the Ketjen carbon (KB) as the catalyst for the cathodes materials. A lesson from the Fig. 5d is that when only the Kb was used as the catalyst, the cycle performance was poor and after 20 cycles only the cutoff potential reached the upper limited potential 4.5 V. So, the amazing cycle performance is mainly owing to the active materials $Cu_2O$.

Figure 6 shows the X-ray diffraction (XRD) pattern of the cathode catalyst materials after 80 cycles. From Fig. 6, it could be seen that the catalyst activity cathode is composed of the $Cu_2O$ as the catalyst activity material, carbon paper and $Li_2O_2$. In addition, the diffraction peaks about the $Li_2CO_3$ can be detected in the XRD pattern also and we suspect that the $Li_2CO_3$ may have come from the decomposition of the electrolyte or the binder during the discharge/charge process. The stable and undecomposed $Li_2CO_3$ was accumulated gradually and would cover the surface and licked up all the active sites of the activity material and eventually lead to the failure of the catalyst materials and the death of the Li-$O_2$ batteries [14, 26, 27].

Good conductivity favors more active substances involved in the electrochemical reaction, which is conducive to improving the specific capacity and cycle stability [28]. Here, the charge transfer impedance of the battery before/after the origin cycle with the current density of 500 mA $g^{-1}$ is displayed in the Fig. 6b. From the diameter of a semicircular, it can be found that the internal resistance is very small and which indicated the as synthesized yolk-shell structured $Cu_2O$ spheres with good catalytic activity.

## Conclusions

In summary, yolk-shell structured $Cu_2O$ spheres were self-assembled with the small $Cu_2O$ nanoparticles which were facilely synthesized with a wet-chemistry method with the PEG-500 as the surfactant.

The fabricated yolk-shell structured $Cu_2O$ indicated a highly porous micro/nanostructure with nanoscale pore size and high specific surface areas. As the cathode catalyst activity materials of the Li-$O_2$ batteries, the novel yolk-shell structured $Cu_2O$ spheres showed a low discharge/charge potential platform of 1.10 or 1.28 V with current density of 200 and 500 mA $g^{-1}$, respectively. Compared with the cycling performance of the cubic-like $Cu_2O$ nanoparticles which were synthesized without the surfactant in this manuscript, the yolk-shell structured $Cu_2O$ spheres indicated a long and stable recycling time of 84 cycles with a high current density of 500 mA $g^{-1}$, which was more than twice of the cycling life of the cubic-like $Cu_2O$ nanoparticles. The outstanding cycling performance of yolk-shell structured $Cu_2O$ spheres results from the special structure and superior ORR/OER catalytic performance. This study would set a novel direction toward the applying of $Cu_2O$ and $Cu_2O$-based nanocomposite as cathode for Li-$O_2$ batteries.

## Acknowledgements

This work was financially supported by K.C. Wong Magna Fund in Ningbo University, Ningbo natural science fund (Project No. 201701HJ-B01019) and college students of science and technology innovation projects in Zhejiang province (Project No. 2017R405008).

## References

[1] Bruce PG, Freunberger SA, Hardwick LJ, Tarascon J-M (2012) Li-$O_2$ and Li–S batteries with high energy storage. Nat Mater 11:19–29

[2] Lu J, Li L, Park J-B, Sun Y-K, Wu F, Amine K (2014) Aprotic and aqueous Li–$O_2$ batteries. Chem Rev 114:5611–5640

[3] Balaish M, Kraytsberg A, Ein-Eli Y (2014) A critical review on lithium-air battery electrolytes. Phys Chem Chem Phys 16:2801–2822

[4] Oh D, Qi J, Lu Y-C, Zhang Y, Shao-Horn Y, Belcher AM (2013) Biologically enhanced cathode design for improved capacity and cycle life for lithium-oxygen batteries. Nat Commun 4:2756

[5] Lim H, Lee B, Bae Y, Park H, Ko Y, Kim H, Kim J, Kang K (2017) Reaction chemistry in rechargeable Li-$O_2$ batteries. Chem Soc Rev 46:2873–2888

[6] Lu J, Jung Lee Y, Luo X, Chun Lau K, Asadi M, Wang H-H, Brombosz S, Wen J, Zhai D, Chen Z, Miller DJ, Sub Jeong Y, Park J-B, Zak Fang Z, Kumar B, Salehi- Khojin A, Sun Y-K, Curtiss LA, Amine K (2016) A lithium–oxygen battery based on lithium superoxide. Nature 529:377–382

[7] Hu X, Li Z, Chen J (2017) Flexible Li-$CO_2$ batteries with liquid-free electrolyte. Angew Chem Int Ed 56:5785–5789

[8] Luo WB, Gao XW, Chou SL, Wang JZ, Liu HK (2015) Porous Ag Pd–Pd composite nanotubes as highly efficient electrocatalysts for lithium–oxygen batteries. Adv Mater 27:6862–6869

[9] Jian Z, Liu P, Li F, He P, Guo X, Chen M, Zhou H (2014) Core–shell-structured CNT@$RuO_2$ composite as a high-performance cathode catalyst for rechargeable Li–$O_2$ Batteries. Angew Chem Int Ed 53:442–446

[10] Ma L, Luo X, Kropf AJ, Wen J, Wang X, Lee S, Myers DJ, Miller D, Wu T, Lu J, Amine K (2016) Insight into the catalytic mechanism of bimetallic platinum–copper core–shell nanostructures for nonaqueous oxygen evolution reactions. Nano Lett 16:781–785

[11] Peng Z, Freunberger SA, Chen Y, Bruce PG (2012) A reversible and higher-rate Li-O2 battery. Science 337:563–566

[12] Liu X, Dai L (2016) Carbon-based metal-free catalysts. Nat Rev Mater 1:16064

[13] Cheng F, Chen J (2012) Metal–air batteries: from oxygen reduction electrochemistry to cathode catalysts. Chem Soc Rev 41:2172–2192

[14] Wang C, Zhao Y, Liu J, Gong P, Li X, Zhao Y, Yue GH, Zhou Z (2016) Highly hierarchical porous structures constructed from NiO nanosheets act as Li ion and $O_2$ pathways in long cycle life, rechargeable Li–$O_2$ batteries. Chem Commun 52:11772–11774

[15] McCloskey BD, Speidel A, Scheffler R, Miller DC, Viswanathan V, Hummelshøj JS, Nørskov JK, Luntz AC (2012) Twin problems of interfacial carbonate formation in nonaqueous Li–$O_2$ batteries. J Phys Chem Lett 3:997–1001

[16] Fu LJ, Gao J, Zhang T, Cao Q, Yang LC, Wu YP (2007) R. Holze b, H.Q. Wu, Preparation of $Cu_2O$ particles with different morphologies and their application in lithium ion batteries. J Power Sourc 174:1197–1200

[17] Xiang JY, Wang XL, Xia XH, Zhang L, Zhou Y, Shi SJ, Tu JP (2010) Enhanced high rate properties of ordered porous $Cu_2O$ film as anode for lithium ion batteries. Electrochim Acta 55:4921–4925

[18] Park JC, Kim J, Kwon H, Song H (2009) Gram-scale synthesis of $Cu_2O$ nanocubes and subsequent oxidation to $Cu_2O$

hollow nanostructures for lithium-ion battery anode materials. Adv Mater 21:803–807

[19] Yue GH, Zhang Y, Zhang XQ, Wang CG, Zhao YC, Peng DL (2015) Synthesis of $Cu_2O$ mesocrystal and its application in photocatalysis. Appl Phys A 118:763–767

[20] Xu H, Wang W, Zhu W (2006) A facile strategy to porous materials: coordination-assisted heterogeneous dissolution route to the spherical $Cu_2O$ single crystallites with hierarchical pores. Micropor Mesopor Mater 95:321–328

[21] Kuo CH, Chu YT, Song YF, Huang MH (2011) $Cu_2O$ Nanocrystal-templated growth of $Cu_2S$ nanocages with encapsulated Au nanoparticles and In-Situ transmission X-ray microscopy study. Adv Funct Mater 21:792–797

[22] Biesingera MC, Laua LWM, Gersonb AR, Smart RSC (2010) Resolving surface chemical states in XPS analysis of first row transition metals, oxides and hydroxides: Sc, Ti, V, Cu and Zn. Appl Surf Sci 257:887–898

[23] Liu L, Wang J, Hou Y, Chen J, Liu HK, Wang J, Wu Y (2015) Self-assembled 3D foam-like $NiCo_2O_4$ as efficient catalyst for lithium oxygen batteries. Small 12:602–611

[24] Tong S, Zheng M, Lu Y, Lin Z, Li J, Zhang X, Zhou H (2015) Mesoporous NiO with a single-crystalline structure utilized as a noble metal-free catalyst for non-aqueous Li–O 2 batteries. J Mater Chem A 3:16177–16182

[25] Liu Q, Jiang Y, Xu J, Xu D, Chang Z, Yin Y, Zhang X (2015) Hierarchical $Co_3O_4$ porous nanowires as an efficient bifunctional cathode catalyst for long life Li-$O_2$ batteries. Nano Res 8:576–583

[26] Cui ZH, Fan WG, Guo XX (2013) Lithium–oxygen cells with ionic-liquid-based electrolytes and vertically aligned carbon nanotube cathodes. J Power Sourc 235:251–255

[27] Park JE, Lee GH, Shim HW, Kim DW, Kang Y, Kim DW (2015) Examination of graphene nanoplatelets as cathode materials for lithium–oxygen batteries by differential electrochemical mass spectrometry. Electrochem Commun 57:39–42

[28] Zhao Y, Li X, Liu J, Wang C, Zhao Y, Yue GH (2016) MOF-derived ZnO/$Ni_3ZnC_{0.7}$/C hybrids yolk–shell microspheres with excellent electrochemical performances for lithium ion batteries. ACS Appl Mater Interfaces 8:6472–6480